# Project 059(B) Jet Noise Modeling and Measurements to Support Reduced LTO Noise of Supersonic Aircraft Technology Development

## Georgia Institute of Technology/Gulfstream

## Project Lead Investigator

Krishan K. Ahuja
Regents Professor
School of Aerospace Engineering
Georgia Institute of Technology
Atlanta, GA 30342
404-290-9873
Krish.Ahuja@ae.gatech.edu

## University Participants

**Georgia Institute of Technology (Georgia Tech)**

- PI: Krishan K. Ahuja, Regents Professor
- FAA Award Number: 13-C-AJFE-GIT-060
- Period of Performance: June 5, 2020 to December 31, 2021
- Tasks:
  1. Form an advisory panel
  2. Identify baseline nozzle requirements and design tests
  3. Design and fabricate a baseline nozzle
  4. Test setup and experimental data acquisition
  5. Data dissemination
  6. Assess readiness of design tools for a simple baseline nozzle configuration
  7. Proposal for a follow-on effort for years 2 and 3
  8. Reporting and data dissemination

## Project Funding Level

This project received $250,000 from FAA and $250,000 of cost-sharing from Gulfstream.

## Investigation Team

- Dr. Krishan Ahuja, PI, Georgia Tech
- Dr. Dimitri Mavris (Co-PI) and Dr. Jimmy Tai (Co-PI), Georgia Tech
- Dr. Aharon Karon, Co-Investigator and Lead Experimentalist, Georgia Tech Research Institute (GTRI)
- Dr. Robert Funk, Experimentalist, GTRI
- David N. Ramsey, Graduate Research Assistant and Experimentalist, Georgia Tech

## Project Overview

The overall goal of this project is to perform cost-effective supersonic transport (SST) jet noise research/technology experiments to enable low-, medium-, and high-fidelity jet noise prediction methods. The specific objective is to design the experiments in collaboration with industry, NASA, the Department of Defense (DOD), FAA, and modelers funded by FAA to help develop improved jet noise prediction methods with reduced uncertainty and enable industry to design quieter supersonic jet engines with higher confidence regarding the noise that will be generated. In collaboration with Gulfstream, Georgia Tech's industry partner on this project, a representative baseline nozzle design will be selected for experiments at

Georgia Tech. The data acquired will consist of far-field noise, high-speed flow visualization, source location, and detailed mean and unsteady flow measurements.

The experimental data acquired by Georgia Tech will be provided to key stakeholders and other computational teams funded by FAA to validate their computational simulations to confirm that jet noise predictions using semi-empirical and computational modeling approaches can be reliably used for jet noise evaluation.

## Task Objectives, Research Approach, and Accomplishments

This project has eight tasks, as listed below. The task titles are self-descriptive and reflect the task objectives. A short objective statement, research approach, and summary of the accomplishments to date for each task is provided after each task description.

## Task 1 - Form an Advisory Panel

Georgia Institute of Technology

### Objective

The objective of this task is to receive regular feedback from industry and NASA subject-matter experts (SMEs) in supersonic jet noise.

### Research Approach

Dr. Liu, the FAA Project Manager for ASCENT 59, has already formed an advisory panel consisting of representatives of FAA, DOD, NASA, Aerion, GE, and Gulfstream. A kick-off meeting has already been held, and feedback from the meeting was used in the design of the test nozzle and determination of the test conditions, as described below.

## Task 2 - Identify Baseline Nozzle Requirements and Design Tests

Georgia Institute of Technology

### Objective

The objective of this task is to define the nozzle requirements and design the experiments.

### Research Approach

The baseline nozzle and tests were based on a paper engine design created by the Georgia Tech Aerospace Systems Design Laboratory (ASDL), guided by ASCENT Project 10, on engine cycle selection for the GT Medium SST (55-passenger class). For simplicity, it was decided that the GT nozzle model tested under this project would not have a plug. For calculation of the area of the outer (secondary flow) duct, the annular areas of the paper engine were used to calculate the area of the secondary flow duct in the model nozzle facility. The GTRI model is at a scale of 0.045 with respect to the paper engine. The mixing length/exhaust nozzle exit diameter ($L_e/D_e$) ratios will be: 0.7, 1, 2, and 3. The contributions of the ASDL are summarized in Appendix A.

As described below, tests have been designed with variations in nozzle design and/or operating parameters to explore the accuracy of semi-empirical and computational tools for predicting jet noise. The test conditions are summarized in Figure 1, which reflects the planned test conditions for each $L_e/D_e$ and each core temperature (unheated and 500 °F). Additionally, PIV, source location, and flow visualization are restricted to unheated set points. Of note, the small extraction ratio (ER) acoustic measurements were acquired with a primary pressure ratio (PR) of 1.69 for all configurations except the $L_e/D_e$ = 1.0 configuration, and the condition with primary pressure of 1.69 and ER of 1.04 was not tested for the shortest mixing duct, $L_e/D_e$ = 0.7. These two caveats arose as a result of the late addition of these conditions with a higher primary pressure ratio, and thus a small ER, to the measurement program.

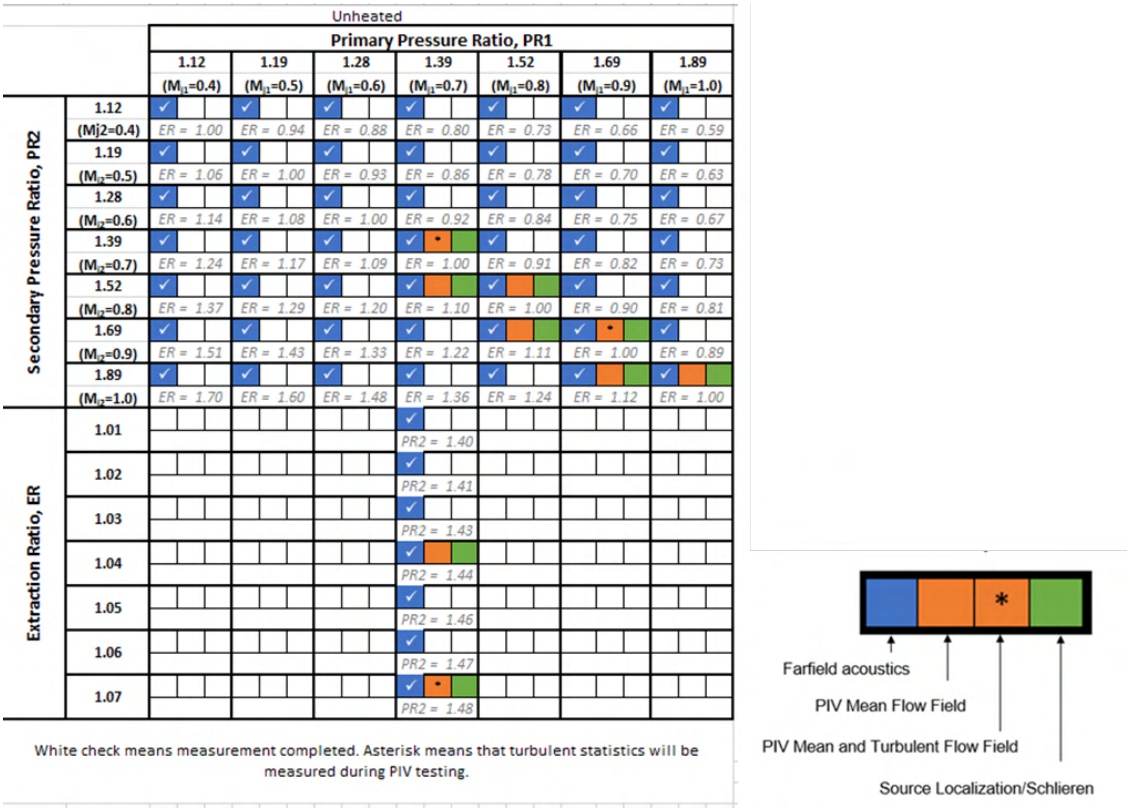


**Figure 1.** Test condition matrix.

## Task 3 - Design and Fabricate a Baseline Nozzle

Georgia Institute of Technology

### Objective

The objective of this task is to design and fabricate a baseline nozzle that meets the requirements defined in Task 2 and is also suitable for the tests required to meet the objectives of the overall program.

### Research Approach

The test nozzle design is shown in Figure 2. A photographic view is shown in Figure 3. The model consists of the following parts: primary nozzle with a collar to avoid any anomalous flow effects due to any geometrical protrusions/recesses, secondary nozzle, mixer ducts, and exhaust nozzle. Three mixer ducts were fabricated to allow for different *mixing length-to-nozzle-exit diameter ratios* ($L_e/D_e$ ratios. The test model utilizes the co-annular flow capabilities of the GTRI jet facilities. The primary and secondary flow streams merge into the mixer-duct and exhaust nozzle combination. The mixer-duct and exhaust nozzle combinations allow for $L_e/D_e$ values of 0.7 (with the exhaust nozzle mounted directly to the secondary nozzle), 1, 2, and 3. The jet stream is ultimately formed by the exhaust nozzle, which is a converging nozzle with geometry based on the converging section of the converging–diverging nozzle from the ASDL engine design.

All components of the test model were fabricated by our Gulfstream cost-sharing partner.

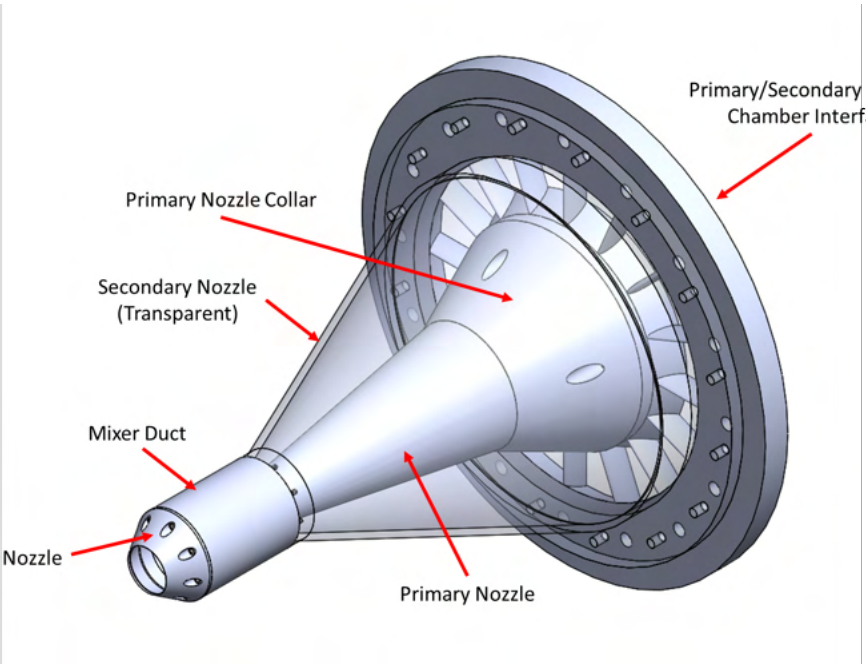


**Figure 2.** Experimental model design.

# Task 4 - Test Setup and Experimental Data Acquisition

Georgia Institute of Technology

## Objective

The objective of this task was to prepare to conduct the tests and acquire and analyze the data. All the acoustic data have been acquired. Because of a major failure in the test facility, as reported in the quarterly progress reports, PIV data could not be obtained earlier. Limited mean flow data were acquired, and the detailed PIV data acquisition is in progress.

## Research Approach

Acoustic Measurements

*Facility Setup and Testing Description*

The test model was mounted in the GTRI Anechoic Jet-Facility for acoustic data acquisition, as shown in Figure 3. This facility has been described in detail in Burrin, Dean, & Tanna (1974), Burrin & Tanna (2005), and Ahuja (2003). Far-field microphones were mounted on a polar arc at angles between 30° and 120° with respect to the jet axis in 10° increments. The jet upstream conditions were set by controlling the ratio of the total pressure to the ambient pressure (PR = $p_t/p_a$) for both the primary and secondary streams. Both the primary and secondary streams were varied between pressure ratios of 1.12 and 1.89. The extraction ratio (ER=$p_{t2}/p_{t1}$) was also used as another approach to define the secondary pressure ratio for a given primary stream pressure, because this parameter was brought to our attention by the program partners and has practical importance. According to insights provided by Gulfstream and FAA, ERs between 1.00 and 1.07 are the most realistic conditions for a given $PR_1$. Additionally, the primary total temperature was set. In the unheated tests, this temperature varied between 60 °F and 70 °F and, during heated tests, it was set nominally to 500 °F. Of note, for the remainder of this program, the PR will refer to the ratio between upstream total and ambient pressures. In addition to the acoustic measurements, the primary and secondary total pressure and temperature, primary and secondary mass flow rates (measured at the control valve), and the ambient pressure, temperature, and relative humidity were measured.

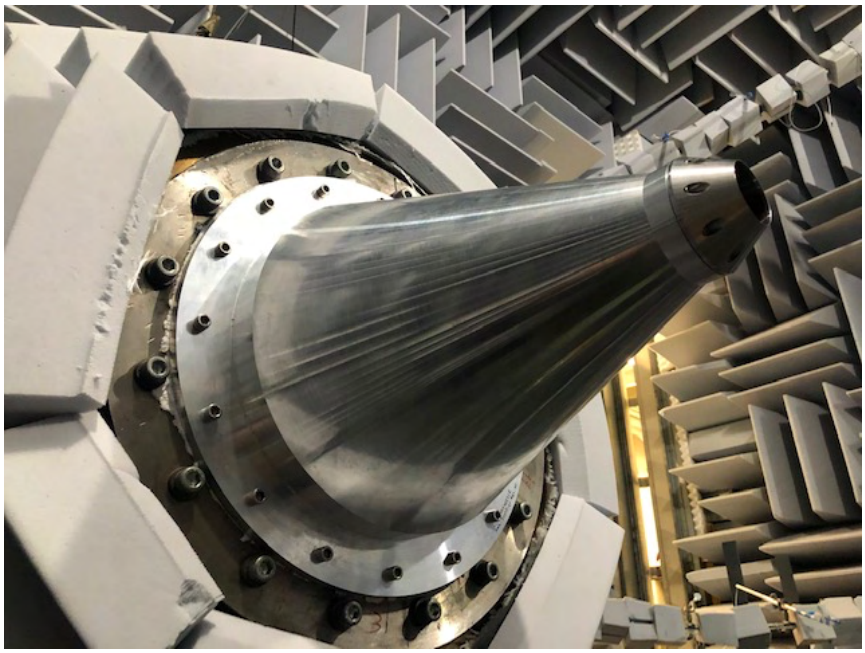

**Figure 3.** Project model setup in the GTRI Anechoic Jet Facility.

The microphones used for these measurements are Bruel and Kjaer (B&K) 4939 ¼-in free-field microphones and are attached to B&K 2669 preamplifiers. The microphone–preamplifier combinations are connected to B&K 2960-A-0S4 Nexus conditioning amplifiers that, in addition to amplifying the signal, act as the microphones' 200-mV power supply. The microphone signals are sampled at 204.8 kHz by using NI PXIe-4499 modules. The acoustic pressure time histories are then processed into averaged sound pressure level (SPL) spectra with a window size of 6,400 samples, 50% overlap, and a Hanning window. To render the data in lossless form for use by the modelers, the following corrections are applied to these SPL spectra: free-field response correction, windsock correction (if necessary), atmospheric attenuation, and distance. These corrections have been described in detail by Karon and Ahuja (2016).

Acoustic Analysis

In the following, only the salient observations are initially provided. Detailed discussion of the results is provided later.

*Effect of changing the Extraction Ratio:* Figure 4 shows the jet noise measurements for jet conditions of ER = 1.1, 1.0, and 0.92 for the $L_e/D_e = 0.7$ configuration. Of note, ER = 1.1 and 0.92 are outside the ER range that the program partners indicated are of greater practical interest; however, the data are shown here because they were acquired as part of this program, and validating the predictions made by the modelers for these conditions would provide added confidence in model fidelity. As shown in Figure 4, the noise increases with increasing secondary pressure ratio. At lower frequencies (below ~3 kHz), the noise increases by ~1 dB as the secondary pressure ratio increases from 1.28 to 1.39 and from 1.39 to 1.52. At higher frequencies, the noise increase is larger. As the secondary pressure ratio is increased from 1.28 to 1.39, the noise increases by as much as 3 dB, and when the secondary pressure ratio is increased from 1.39 to 1.52, the noise increases by as much as 5 dB. Later, we show that if the extraction ratios are maintained close to unity, e.g., up to 1.07, there is no noticeable change in SPLs at low frequencies, and there is very little change at high frequencies.

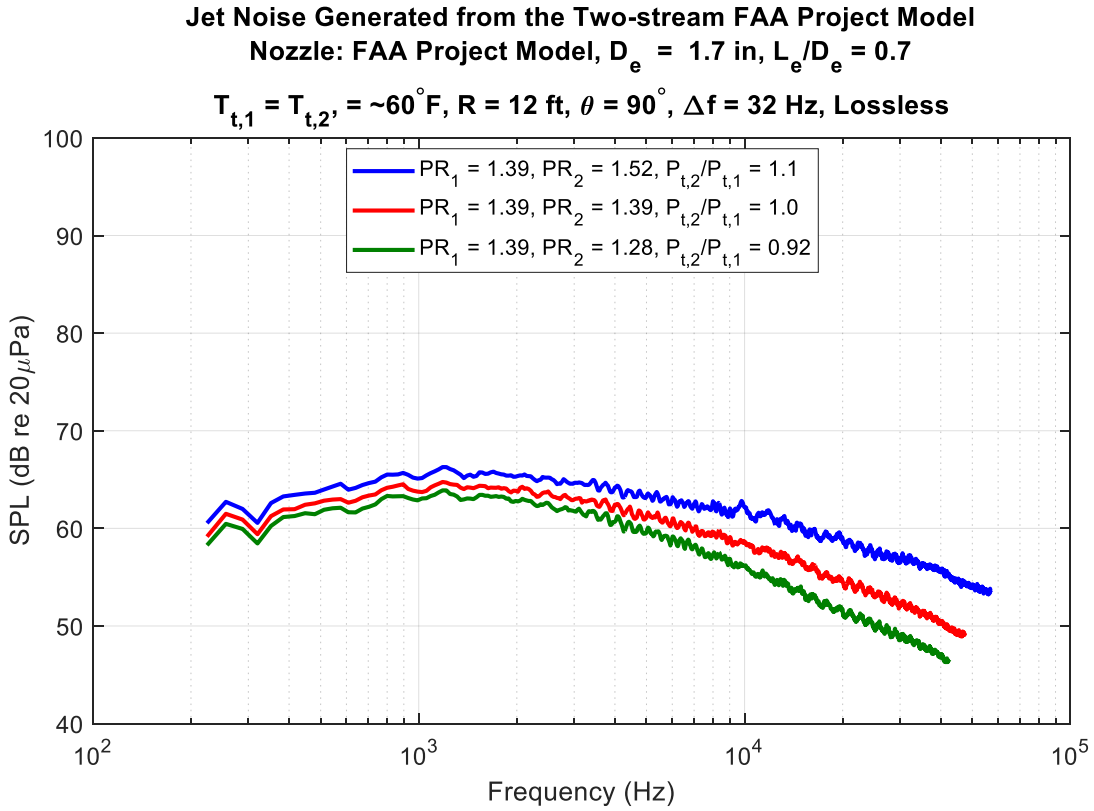


**Figure 4.** Typical jet noise spectra at an extraction ratios of 1 and above and below 1, for the $L_e/D_e$ = 0.7 configuration.

*Effect of increasing the mixing length:* Figure 5 shows the jet noise generated from the test model with primary and secondary pressure ratios both equal to 1.39 (ER = 1.0) and $L_e/D_e$ varied between 0.7 and 3.0. As shown in Figure 5, at frequencies below 7 kHz, the noise from the three conditions is the same. Above 7 kHz, there is a minor reduction in jet noise of 1 dB at most. This result indicates that an increase in mixing length does increase the mixing to a small degree, thus leading to reduced noise at high frequencies.

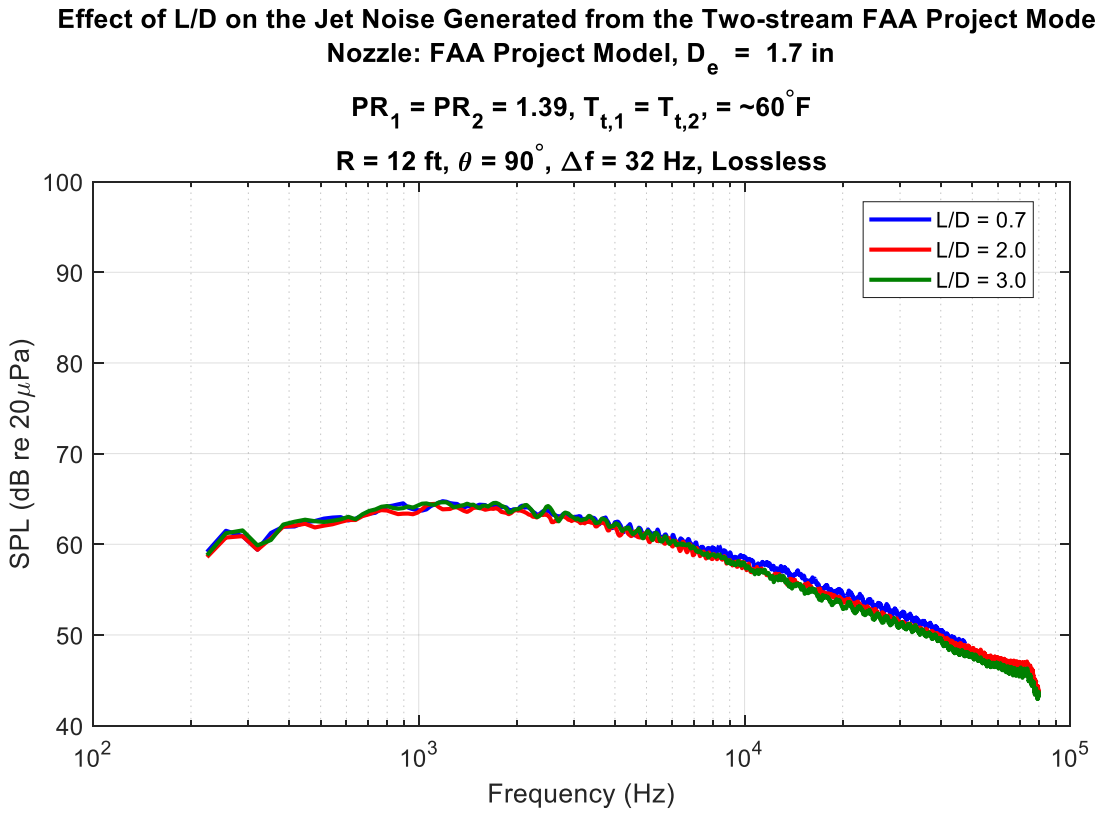


**Figure 5.** Effect of mixing length on the jet noise produced by the test model.

*Effect of increasing the primary jet temperature:* Figure 6 shows the effect of increasing the primary nozzle total temperature for an $L_e/D_e$ of 0.7. The corresponding data for an $L_e/D_e$ of 3 is shown in Figure 7. The unheated spectra in both cases appear to be unaltered, but the spectrum for the larger $L_e/D_e$ with the heated primary stream has somewhat lower SPLs at higher frequencies. For example, at a frequency of 50000 Hz, the SPL for $L_e/D_e$ = 0.7 is 51 dB, and that for $L_e/D_e$ = 3 is 47.4 dB. This finding may be an effect of reduced speed of the heated stream via mixing with the unheated secondary jet in the longer duct.

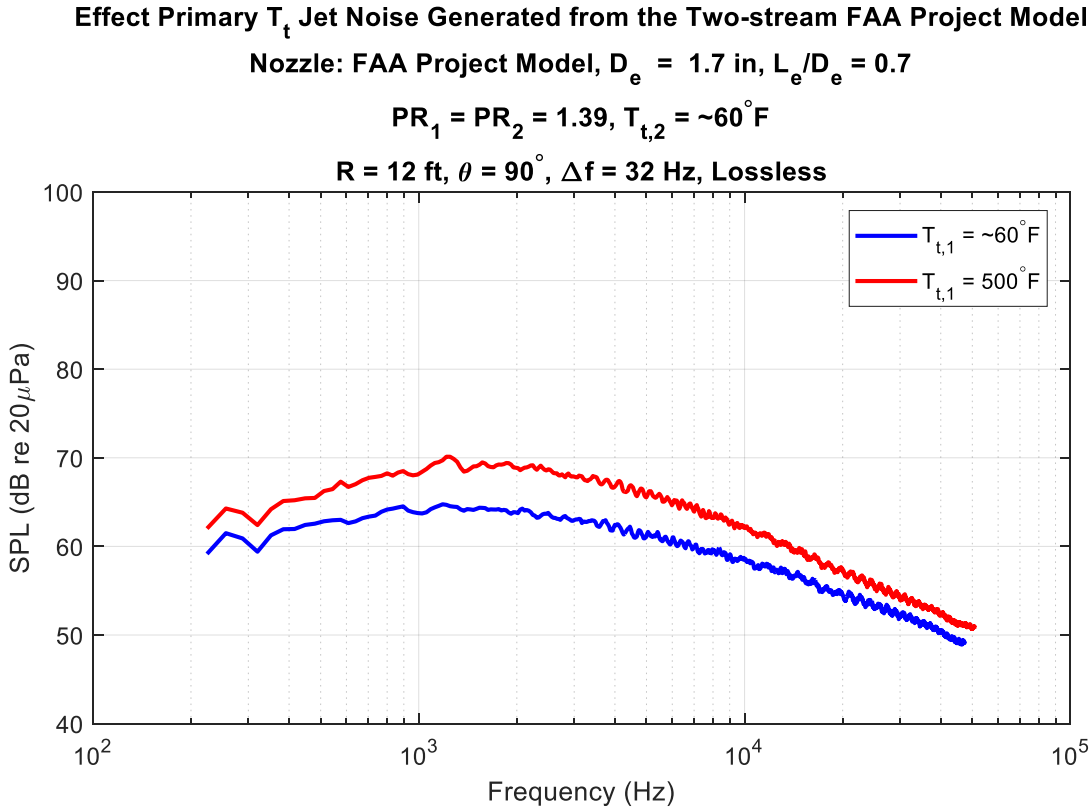


**Figure 6.** Effect of primary total temperature with the $L_e/D_e$ = 0.7 configuration.

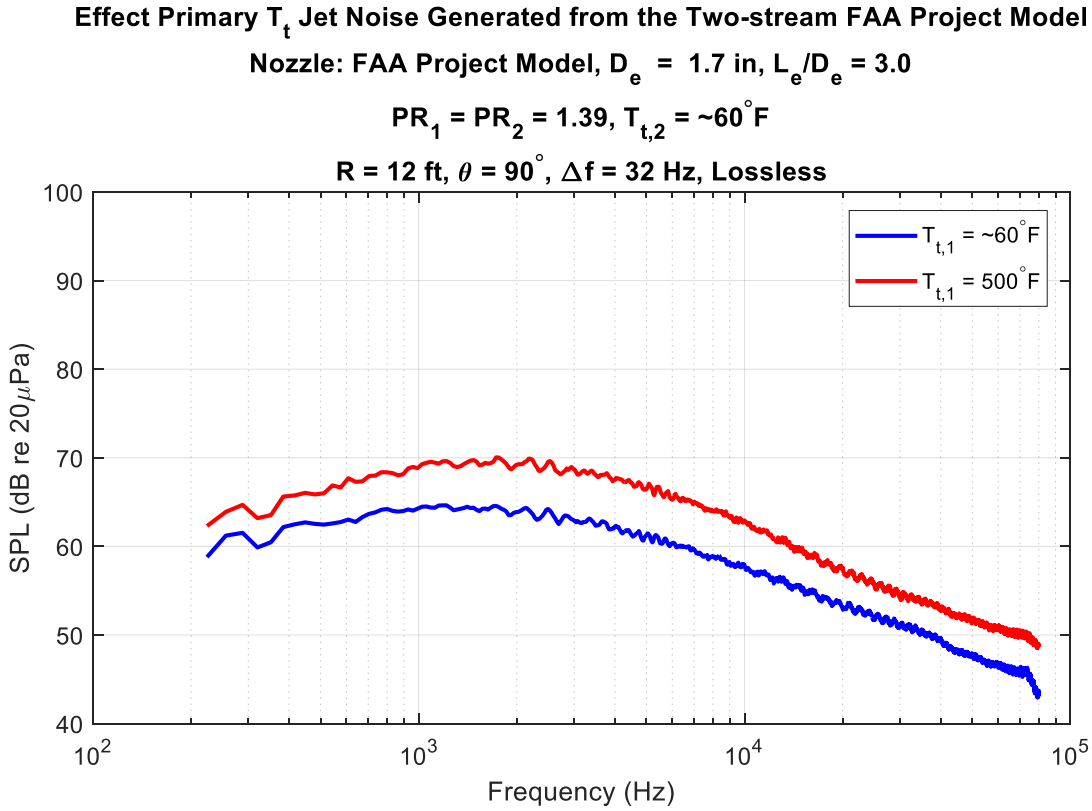


**Figure 7.** Effect of primary total temperature with the $L_e/D_e$ = 3.0 configuration.

*Observation of high-intensity tones at certain operating conditions:* Figures 8 and 9 compare the jet noise measurements for the $L_e/D_e$ = 0.7 and 3.0 configurations for ER = 1.0, and ERs much higher (1.22) and much lower (0.81) than unity. High-amplitude tones are generated for both these cases. An initial analysis and literature review performed by the ASCENT 59B team has led to the hypothesis that these tones may be due to a family of flow-acoustic interactions rather than to a single underlying physical mechanism. The suspected types of flow-acoustic interactions include: (1) the excitation of acoustic resonances inside the model by ducted vortex shedding, which may exist in the wake of the primary nozzle lip inside the mixing duct (2) aeroacoustic feedback, which occurs between the primary nozzle and exhaust nozzle lips, and (3) coupling between the feedback and duct resonances associated with various passages and impedance boundaries within the supply duct. The experimental evidence supporting this hypothesis includes a drop in the fundamental tone frequency that occurs when the internal mixing length exceeds a certain value for a given test point. However, without dedicated experimental evidence, this possibility remains purely a hypothesis. One challenge that arises in distinguishing the two physical mechanisms from far-field acoustic measurements alone is the tendency for both the feedback frequency and acoustic duct modes to decrease in frequency with an increase in mixing duct length (under the assumption that the acoustic mode is not purely transverse and involves the region inside the mixing duct). Although no concrete conclusions can currently be reached, a brief discussion of potential flow-acoustic interactions and how they are believed to relate to the year 1 model is provided below.

Generally, flow over a plate in a duct may excite the duct's acoustic resonances as the plate's trailing edge vortex shedding feeds energy into the acoustic field (Parker & Stoneman, 1989; Cumptsy & Whitehead, 1971). The influence of the excited duct resonance on the vortex street, which excited it, must also be considered. For instance, the most preferred frequency of vortex shedding from a plate inside a duct has been shown to "lock in" on the frequency of an acoustic mode that it has excited (Parker & Stoneman, 1989). This effect is significant when the pressure node of an acoustic resonance coincides with the vortex street's location (Parker & Stoneman, 1989). This phenomenon is not simply due to unsteady flow features exciting duct resonances, and the influence of the acoustic field on the unsteady flow field must also be considered. In the test model

used during year 1, if the frequency of the vortex shedding from the primary nozzle lip matches any of the duct resonance frequencies within the model, high-amplitude tones can result.

Regarding the feedback phenomenon, the low-bypass internally-mixed model used has a primary nozzle diameter comparable to that of the exhaust nozzle, thus forming a geometry that enables the onset of an aeroacoustic feedback phenomenon internal to the model. The feedback phenomenon initiates in the model when a core-bypass shear layer instability wave impinges on the exhaust nozzle lip and produces sound. As the sound propagates upstream to the primary nozzle lip with proper phase, it excites the core-bypass shear layer instability, and the feedback loop is set up. The excited instability wave impinges on the exhaust nozzle lip with greater intensity, higher amplitude sound is produced, and the instability is further reinforced. As this repeats, large oscillations ensue at the feedback frequency and high-intensity tones are produced. It can be shown that an increase in distance between the primary and exhaust nozzle lips tends to reduce the feedback frequency. If the feedback tones match any of the duct resonance frequencies within the test model, tones with even higher amplitude can result. The worst-case scenario occurs when the frequencies associated with vortex shedding, feedback, and duct resonance all match. This scenario could produce structural failures due to sonic fatigue.

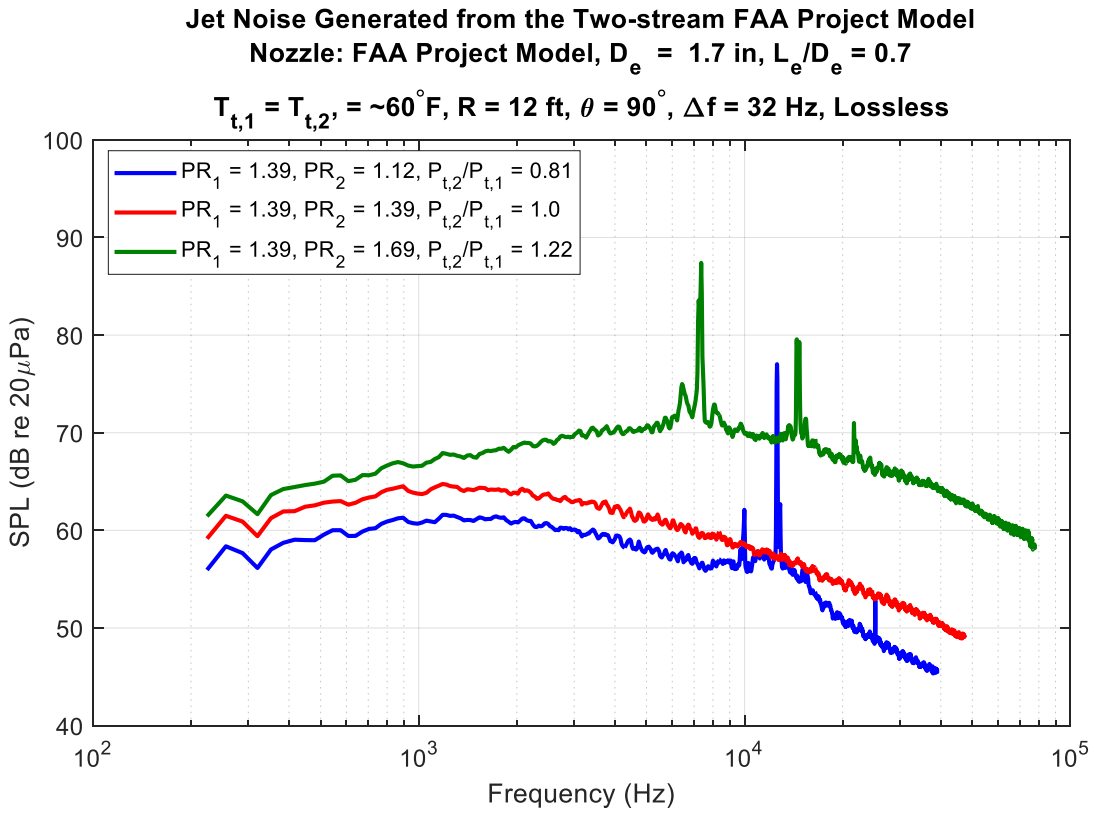


**Figure 8.** Jet noise measurements with pressure splits far from unity for the $L_e/D_e$ = 0.7 configuration.

The large shift in the tone's fundamental frequency from ER = 1.22 to ER = 0.81 (Figure 8) is believed to represent a change in the underlying physical mechanism responsible for the tones, perhaps because of a change from the resonances excited by the ducted core-bypass vortex to the feedback phenomenon. Using bracketing assumptions that the convection speed of an instability wave inside the model is similar to that of a free jet, and that the two streams have approximately reached their full flow velocities before reaching the mixing duct inlet, the predicted feedback frequencies are much less than 6 kHz. This finding suggests that the tones in Figure 8 and in the upper spectrum shown in Figure 9 are unlikely to be due to feedback occurring between the primary and exhaust nozzle lips. The predictions are not sufficiently sensitive to the assumed instability wave convection speed for invalidity of the assumed value to provide a possible explanation for the differences between the measured high-frequency tones and the expected relatively low-frequency feedback tone. Furthermore, for a

given test point ($PR_1$ = 1.39, ER = 0.88), switching between the shortest and longest mixing duct configurations causes the tone's fundamental to jump to a much lower frequency. This is consistent with expectations for the emergence of a feedback phenomenon; namely, that there is a minimum mixing duct length for which the core-bypass shear layer instability has adequate time to grow during its convection inside the mixing duct before impingement on the exhaust nozzle lip. If the tones are due to a feedback phenomenon, when the sound wave travels from the exhaust nozzle toward the primary nozzle lip, it will take longer for the extraction ratio of 1.22 than for 0.81, because the higher-speed flow of the outer steam will slow the sound travel time to the primary nozzle to a greater extent. This will reduce the feedback frequency. Likewise, the instability wave will travel downstream slowly, because the relative velocity of the primary jet will be lower. This aspect will also contribute to the reduction of the final feedback frequency for the higher extraction ratio as seen here.

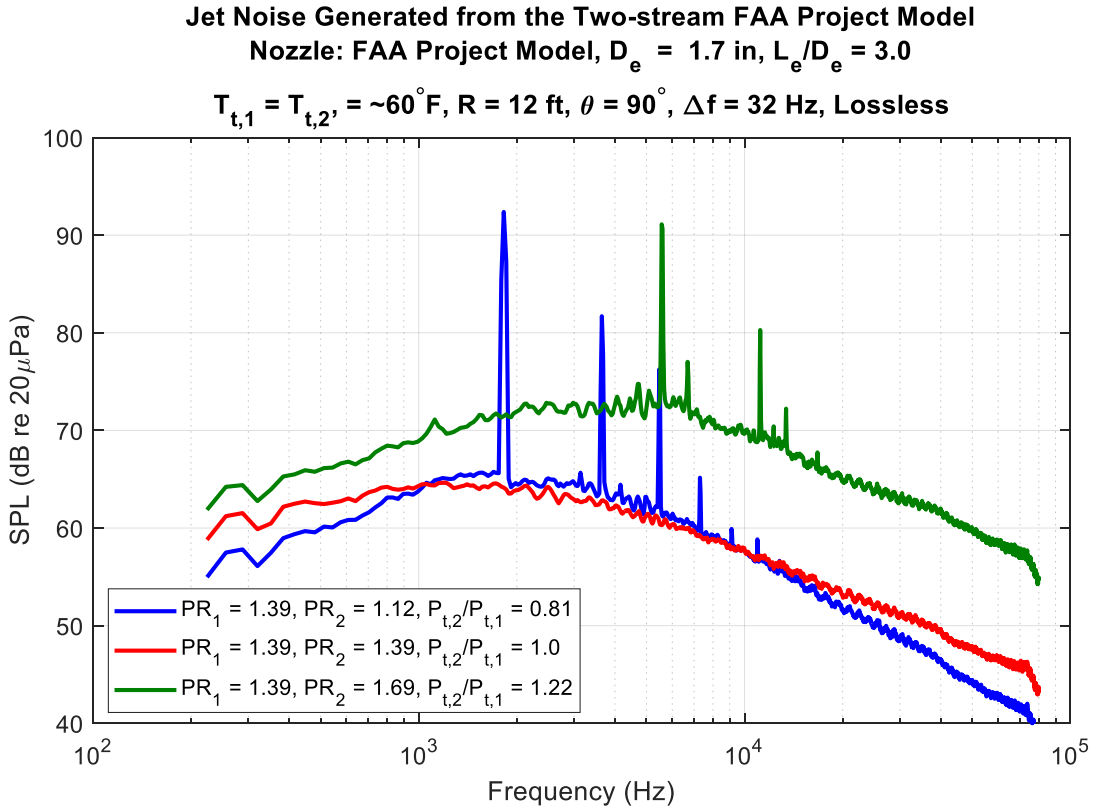


**Figure 9.** Jet noise measurements with pressure splits far from unity for the $L_e/D_e$ = 3.0 configuration.

Figure 10 shows a comparison of the noise produced with the $L_e/D_e$ = 3.0 configuration when $PR_1$ = $PR_2$ = 1.39 vs. that produced when only the primary stream is set to $PR_1$ = 1.39 and the secondary stream is closed off. Figure 11 shows the corresponding centerline velocity profiles. Ideally, an effect of a small change in diameter should be observed. That is, we assume that the case in which the primary nozzle is operating at $PR_1$ = 1.39 and the secondary stream is closed off is associated with a primary nozzle diameter of 1.6 in, and that the case of the primary and secondary stream operating at $PR_1$ = $PR_2$ = 1.39 is associated with the exhaust nozzle diameter of 1.7 in. This increase in diameter should cause an increase in low-frequency noise and a decrease in high-frequency noise when SPL is plotted as a function of frequency. When SPL is plotted as a function of Strouhal number, a constant noise increase should be observed across the entire spectrum. In this case, the nozzle diameters are nearly identical (1.6 in for the primary vs. 1.7 in for the exhaust nozzle). This would result in a theoretical 0.53 dB increase and a negligible frequency shift, if a plug flow profile is assumed at the exit of the exhaust nozzle. The above argument is presented to understand what factors would increase the low frequency and to emphasize the finding of only minor changes in peak frequency shift and changes in SPLs due to the geometry used. We are unable to determine what the internal mixing will do, except that the high-frequency noise produced near the primary nozzle exit will be partly shielded by the ducting.

However, as shown in Figure 10, when only the primary stream is active, tones are produced by the model, and the two cases exhibit large noise level differences, because operating the primary nozzle alone with the secondary ducting in place creates an acoustically excited jet. This excitation causes broadband noise amplification, as discussed by Ahuja and Blakney (1985) and Lepicovsky et al. (1985). Figure 11 shows a significant shortening of the potential core in the case of the primary nozzle operating with the secondary stream closed off, which is a characteristic of a tone-excited jet. Of note, these tones are produced inside the nozzle ducting and therefore will be much louder than measurements in the far field. As shown in Figure 10, these tones are absent in the case of the primary and secondary streams operating at the same pressure ratio. As shown below, this effect reappears at higher pressure ratios (possibly because of a mismatch in feedback frequencies and duct resonance frequencies). The feedback frequency will change as the speed of sound for the return path of the feedback is reduced by the secondary stream, as shown by Lepicovsky and Ahuja (1985). In the future, a more exact explanation is anticipated, but the modeling teams should be able to predict this effect.

This measurement also confirms a correlation between the tones and a large change in the flow field. To be certain that the change in potential core length is a tone-induced effect, as assumed in the explanation above, the potential core length for a given primary pressure ratio and a wide range of different secondary pressure ratios must be measured. The primary pressure ratio should be selected such that no tones are produced when the primary and secondary pressure ratios are matched. If, at some change in secondary pressure ratio, tones emerge, and a simultaneous decrease in the potential core length is observed, the potential core shortening can be assumed with greater confidence to be due to the tone and to be part of a flow-acoustic interaction. The detailed PIV flow-field measurements to be conducted by the end of year 1 will provide greater insight into the link between the tones and changes in the flow field.

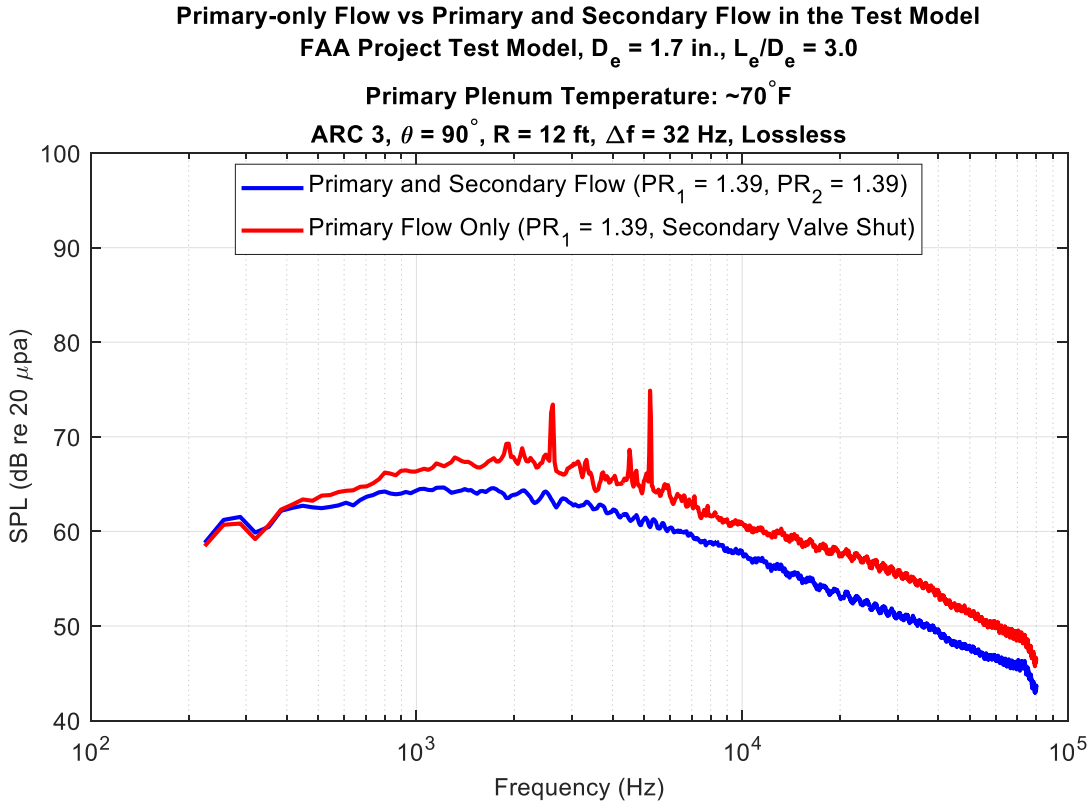


**Figure 10.** Comparison of the noise produced by the test model with $L_e/D_e$ = 3.0, when $PR_1 = PR_2$ = 1.39 vs. only an active primary stream with $PR_1$ = 1.39.

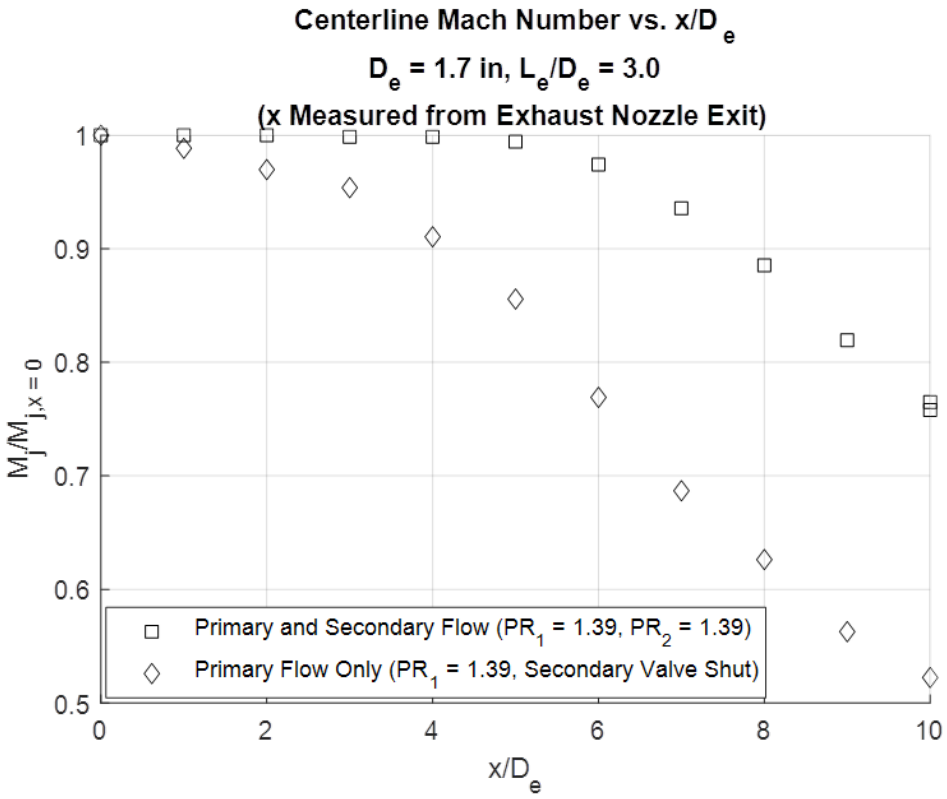


**Figure 11.** Centerline Mach number profile comparison of the jet produced by the test model with $L_e/D_e$ = 3.0 and $PR_1$ = $PR_2$ = 1.39 vs. only an active primary stream with $PR_1$ = 1.39.

*Refined Analysis of Data at Extraction Ratios between 1 and 1.07*

As mentioned above, FAA and Gulfstream indicated that for mixed flow engines the extraction ratio values between 1.00 and 1.07 are the most realistic. Acoustic measurements focusing on this extraction ratio range are presented here. Figure 12 shows the results of the small variations of extraction ratio for a $PR_1$ = 1.39. Figure 12 shows the results as the extraction ratio is varied in steps of 0.01 from 1.00 to 1.07 at a polar angle of 90°. Figure 12 also shows cases of $L_e/D_e$ of 0.7 and 0.3, as well as cases of unheated core flow and core flow heated to 500 °F. Comparisons of Figures 12a and 12b, as well as Figures 12c and 11d, provide some insight into the effect of heating the core flow. There are two main effects from heating the core flow: (1) the overall noise levels increases, as a result of higher jet velocities in the case of heated core flow, and (2) the jet noise spectra show greater collapse. To illustrate the first effect, for both the $L_e/D_e$ = 0.7 and 3.0 cases, the peak noise increases by 5 as the core flow is heated to 500° F. To illustrate the second effect, for both $L_e/D_e$ = 0.7 and $L_e/D_e$ = 3.0, for the unheated case there is a 1-dB difference in the spectra at low frequencies, but this spread increases to 5 dB at high frequencies. For the heated core case, the spectra collapse below 8 kHz, and above 8 kHz all SPLs are within 2 dB. Of note, for the $L_e/D_e$ = 3.0 case, the heated core flow shows very minimal variation in spectral levels. Regarding the effect of mixing length, for the unheated case, the spread in spectral levels is reduced by a maximum of 5 dB to 3 dB. In the heated core flow case, spectral differences above 8 kHz nearly disappear in the $L_e/D_e$ = 3.0 case.

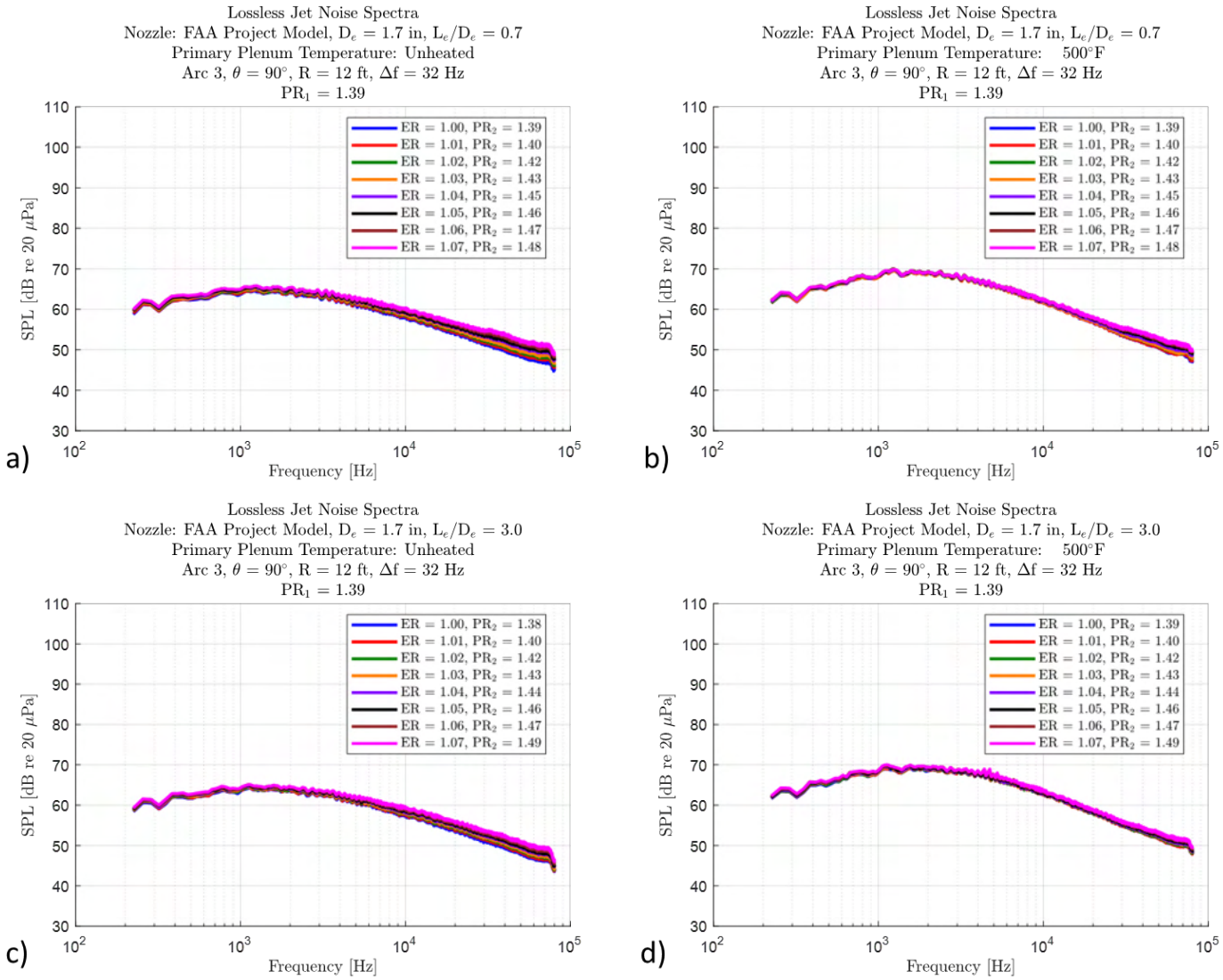


**Figure 12.** Example acoustic measurements for small extraction ratioER changes for PR1 = 1.39 at θ = 90°. (a) $L_e/D_e$ = 0.7 and core flow unheated, (b) $L_e/D_e$ = 0.7 and core flow heated to 500 °F, (c) $L_e/D_e$ = 3.0 and core flow unheated, and (d) $L_e/D_e$ = 3.0 and core flow heated to 500 °F.

Figure 13 shows the same type of acoustic measurements as Figure 12, but for $PR_1$ = 1.69. The above comments regarding the effects of heating the core flow and the change in mixing length again apply. The main difference in the data between Figures 12 and 13 is the presence of tones in the spectra with the $PR_1$ = 1.69. For this primary pressure ratio, tones exist even at an ER = 1.00. As can be seen in Figure 13, with the exception of Figure 13d, the tone level and frequency increase with increasing extraction ratio. Observing the effect of heating the core flow, the tone levels decrease by as much as 10–15 dB in some cases with heating of the core flow. In the unheated condition, increasing the mixing length can increase the tone levels by as much as 10 dB. For the heated condition, as shown in Figure 13d, the increased mixing length actually minimizes the tonal levels.

Importantly, for the cases discussed above, if the tones could be eliminated, there is little difference in the spectral levels primarily to the left of the spectral peak and immediately to the right of the peak, as long as the extraction ratios are maintained close to unity, on the order of 1.07. This result implies that for a fixed primary operating pressure ratio,

increasing the secondary pressure ratio would provide an increase in thrust but add no additional noise at most frequencies of interest. We believe that the presence of the mixer nozzle would eliminate the tones. This phenomenon has been observed very clearly with chevrons and tabs in past work and is attributable to reducing the growth rate of the instability waves—one leg of the feedback phenomenon that we believe is producing the tones. Some answers are expected to be found by approximately March 2022.

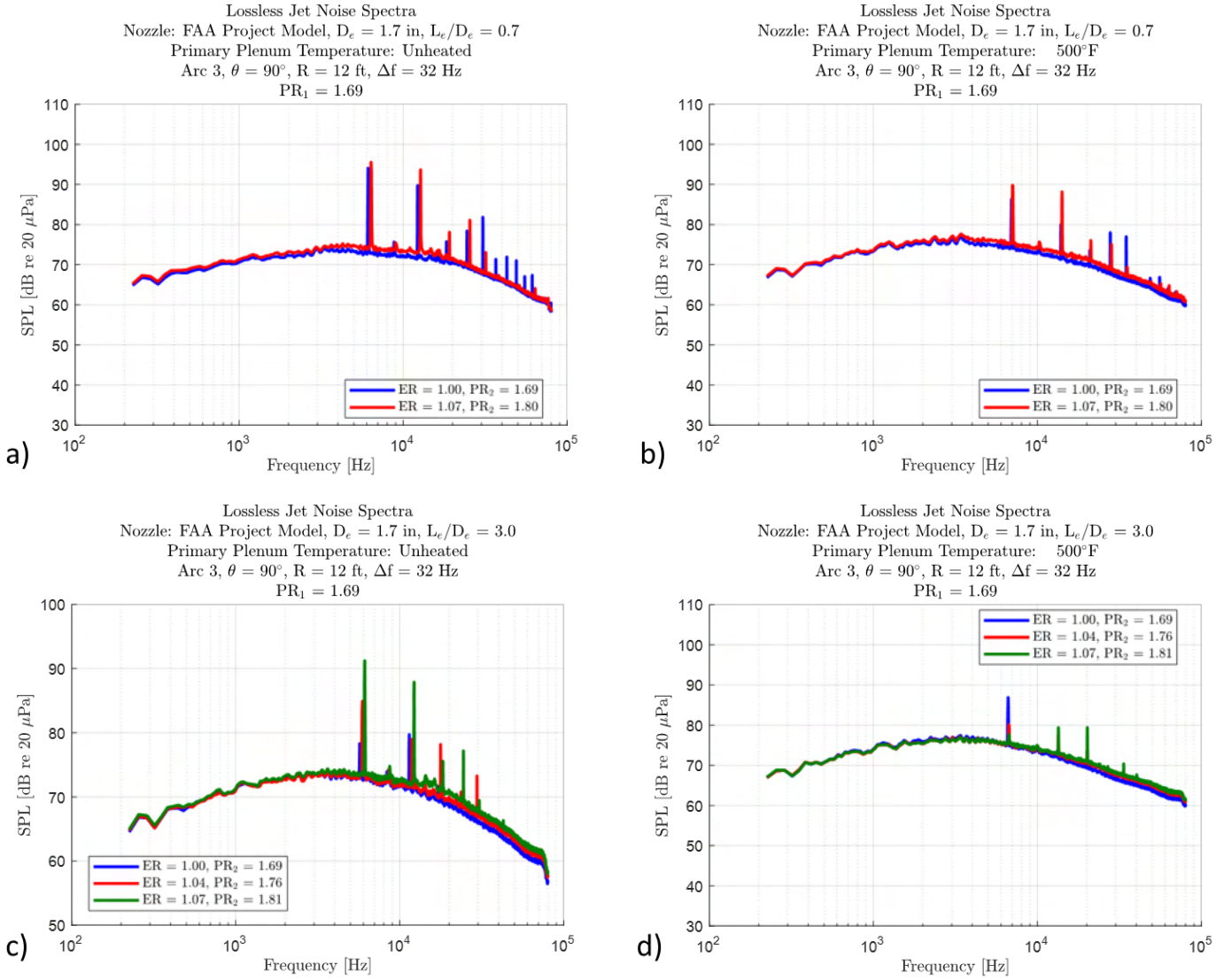


**Figure 13.** Example acoustic measurements for the small extraction ratio changes for PR1 = 1.69 at θ = 90°. (a) $L_e/D_e$ = 0.7 and core flow unheated, (b) $L_e/D_e$ = 0.7 and core flow heated to 500 °F, (c) $L_e/D_e$ = 3.0 and core flow unheated, and (d) $L_e/D_e$ = 3.0 and core flow heated to 500 °F.

*PIV Flow-Field Measurements*

*Methodology:* The jet flow field issued from the model-scale nozzle is characterized by using a double-pulsed PIV system in GTRI's Flow Diagnostics Facility. Details of this facility have been presented by Burrin and Tanna (2005). The instrumentation and hardware in the Flow Diagnostics Facility are shown schematically in Figure 14. The PIV measurements are used to produce mean and unsteady velocity vector fields. These two vector fields are produced for two different physical regions in the jet flow field: (1) a high-spatial-resolution, zoomed-in view of the exhaust nozzle shear layer very close to its exit and (2)

a multi-station traverse, which captures ($0 < x < 20D_e$) by positioning the camera at several stations along the jet axis and stitching the fields measured at each station together. Neighboring stations along the traverse have some viewing-window overlap. In this overlapping region, the vector fields calculated from the station furthest from the nozzle are reported.

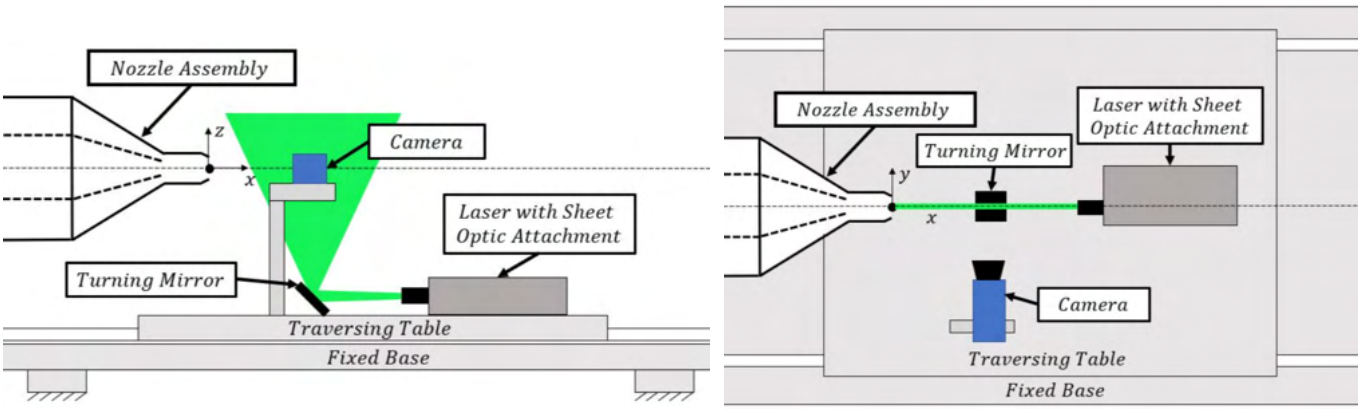


**Figure 14.** GTRI's Flow Diagnostics Facility: (left) side view and (right) top view.

*Validation:* A major focus of the experimental work has been to ensure that the measurements, particularly turbulence statistics, produced by the PIV system are accurate, in accordance with the program's objective to provide valuable, detailed turbulence measurements to modelers. To validate the PIV system setup and data-processing settings, the 1.6-inch conical primary nozzle was installed in isolation in the Flow Diagnostics Facility, as shown in Figure 15. PIV data were acquired for a jet Mach number of 0.58. This approach enabled comparison to the historical data published by Ahuja et al. (1982), which were acquired in the same facility with the same size nozzle. The historical data include mean velocity and turbulence intensity profiles along the jet's centerline and lipline. For this validation run, 750 image pairs were acquired at a nominal rate of 5 Hz and processed. This number of image pairs has been shown to provide acceptable convergence of turbulence intensity measurements during validation work. The two-dimensional mean velocity and turbulence intensity fields measured with the present setup are shown in Figure 16. In this work, the turbulence intensity is given as

$$\mathrm{TI} = \sigma_u / \bar{u}$$

where $\sigma_u$ is the local standard deviation of the $x$-component of velocity. At all points, the turbulence intensity is calculated by normalizing the local $\sigma_u$ by the mean velocity along the jet's centerline at $x/D_e = 0.5$. For mean velocity fields, the local mean velocity is normalized by the mean velocity at the jet's centerline at $x/D_e = 0.5$ as well. The locations in the two-dimensional fields at which to extract lipline and centerline profiles are shown by the black dashed lines in Figure16. Figures 17–19 show the profiles of these fields along the jet's centerline and lipline. In these plots, the solid black curves are 100-point median-filtered curves, whereas the light-gray curves are the true PIV processing outputs. The plot axis limits for velocity profile plots are those used by Ahuja et al. (1982), for ease of visual comparison. The centerline and lipline profiles show excellent agreement with the historical data and provide confidence in both the physical system and the PIV processing settings.

**Figure 15.** The 1.6-in primary nozzle installed in isolation for PIV measurement validation.

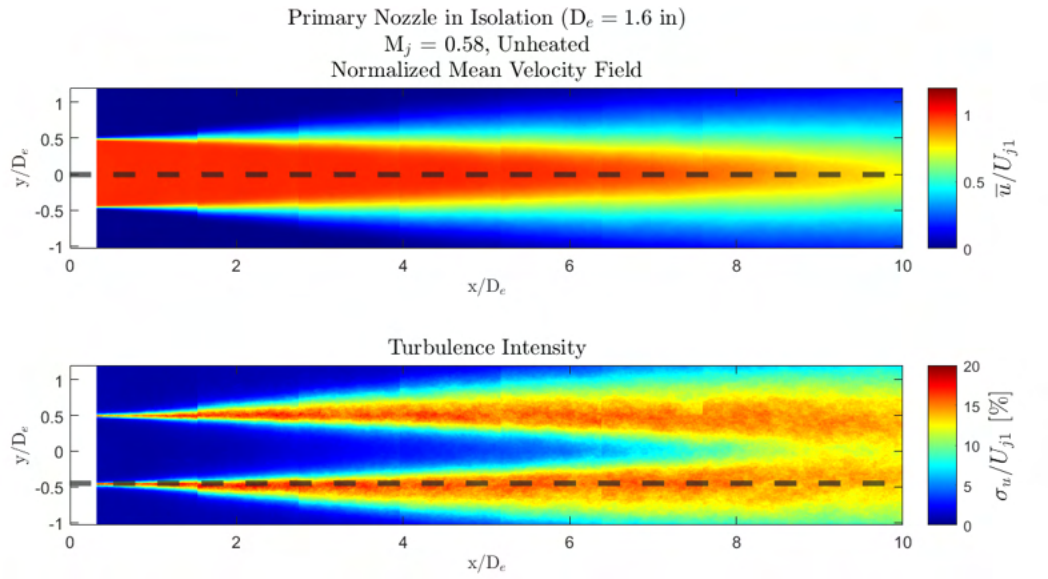


**Figure 16.** Validation dataset's mean velocity (top) and turbulence intensity (bottom) fields.

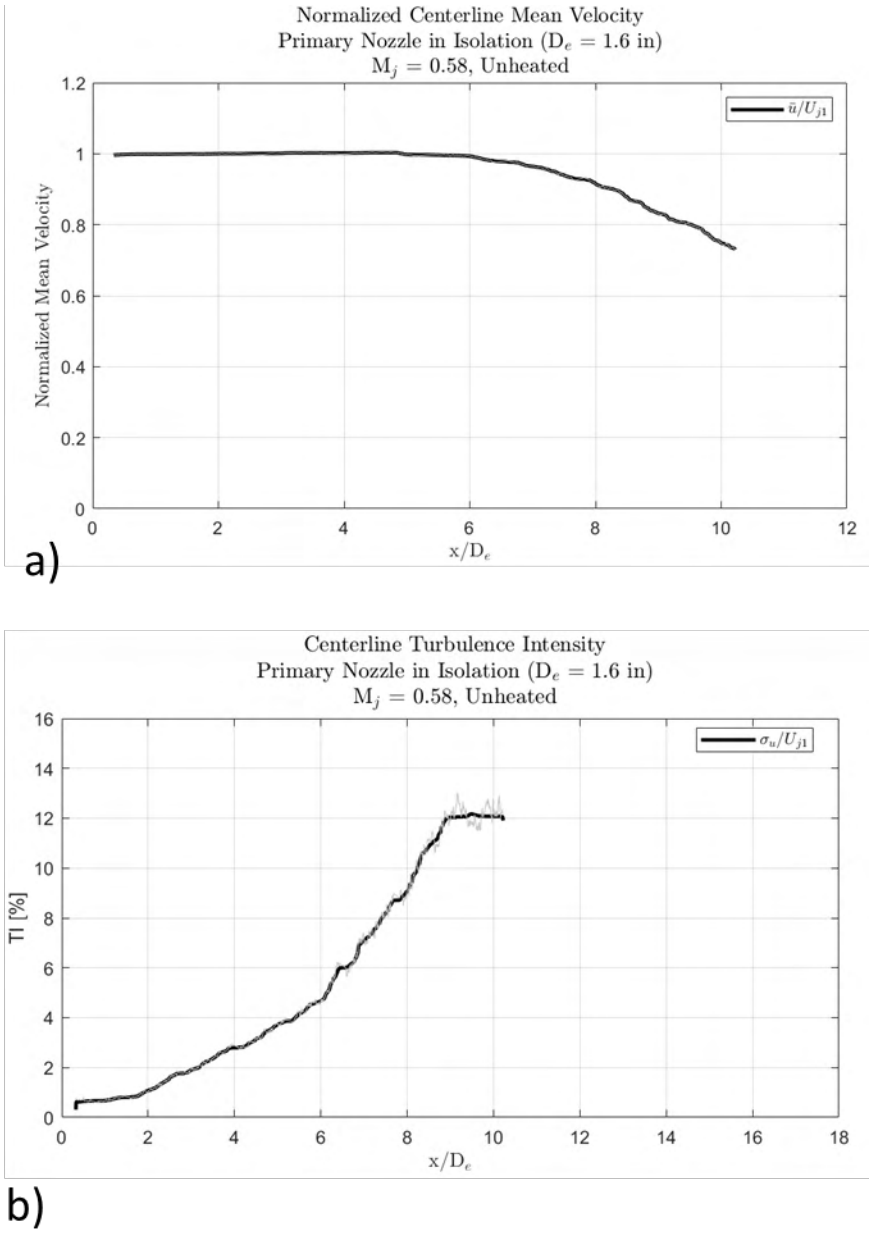


**Figure 17.** Validation of the dataset's (a) centerline mean velocity distribution and (b) centerline turbulence intensity distribution.

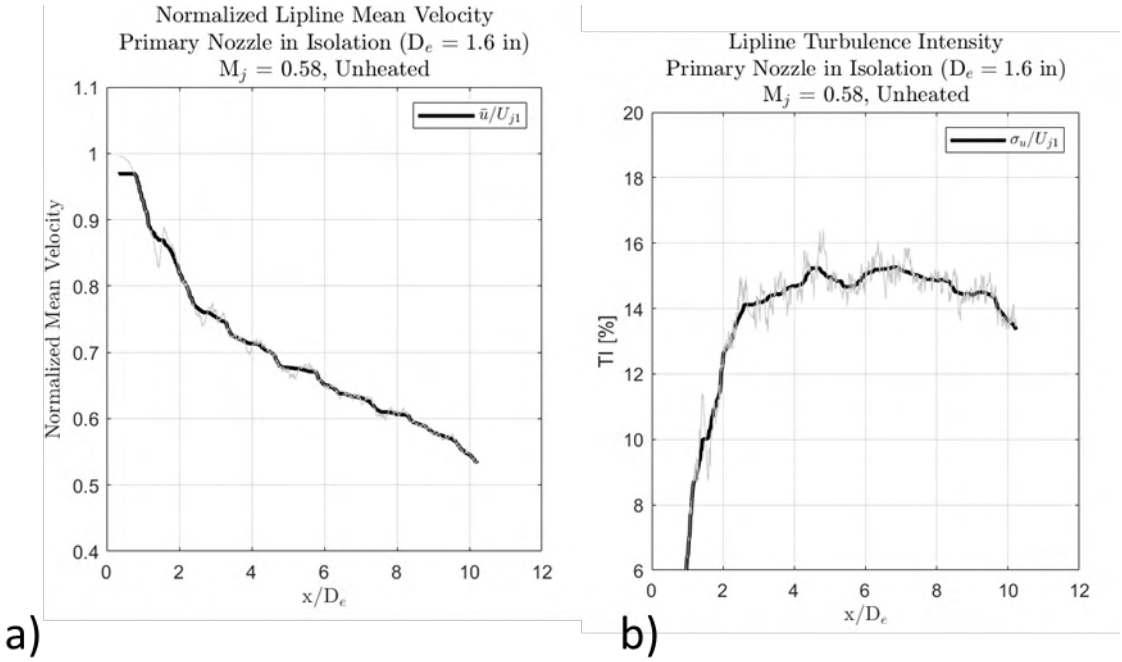


**Figure 18.** Validation of the dataset's (a) lipline mean velocity distribution and (b) lipline turbulence intensity distribution.

## Task 5 - Data Dissemination

Georgia Institute of Technology

### Objective

The objective of this task is to maintain contact with the modelers being funded by FAA under Project 59 and provide them with the nozzle design, and both the acoustic and flow data from the current project.

### Research Approach

The modelers were all informed of our preliminary design during the first Advisory Panel discussion. We have now provided the finalized design to the modelers.

The modelers were provided with boundary-layer and acoustic measurements generated with the primary nozzle acquired for A. Karon's PhD thesis (2016)

At the end of this year, the FAA gave permission to begin the data dissemination. This process had begun with a few conditions, but more should be available in the near future.

## Task 6 - Assess Readiness of Design Tools for a Simple Baseline Nozzle Configuration

Georgia Institute of Technology

### Objective

Whereas Task 5 involves only providing the data to the modelers, the objective of this task is to interact with the modelers in terms of verification of their codes with the measurements made under this project at Georgia Tech. Our partners Gulfstream and ASDL will also be comparing their low-fidelity codes with our data. Georgia Tech is still waiting for the modelers to be ready for acoustic data comparisons.

## Task 7 - Proposal for a Follow-on Effort for Years 2 and 3

Georgia Institute of Technology

The year 2 proposal was submitted at the end of March.

## Task 8 - Reporting and Data Dissemination

Georgia Institute of Technology

All quarterly reports and the 2020 annual report were submitted. Progress was presented at both the Spring and Fall FAA ASCENT Advisory Committee meetings.

### Milestones

The experimental model was designed and fabricated.

All acoustic measurements have been acquired.

### Major Accomplishments

The experimental model was designed and fabricated. All acoustic measurements have been acquired.

### Publications

None

### Outreach Efforts

None

### Awards

None

### Student Involvement

David Ramsey assisted with the design of the experimental model and prepared the documents that were sent to the machine shop. He will continue to be the graduate research assistant on this project.

### Plans for Next Period

- Complete flow measurements
- Prepare for year 2 efforts

### References

Ahuja, K. K. (2003). Designing clean jet-noise facilities and making accurate jet-noise measurements. International Journal of Aeroacoustics, *2*(3), 371-412.

Ahuja, K. K., Lepicovsky, J., Tam, C. K. W., Morris, P. J., & Burrin, R. H. (1982). Tone-excited jet: Theory and experiments (Report No. 3538). National Aeronautics and Space Administration.

Ahuja, K. K., & Blakney, D. F. (1985). Tone excited jets - part IV: Acoustic measurements. Journal of Sound and Vibration, *102*(1), 93-117.

Burrin, R. H., Dean, P. D., & Tanna, H. K. (1974). A new anechoic facility for supersonic hot jet noise research at Lockheed-Georgia. The Journal of the Acoustical Society of America, *55*(2), 400.

Burrin, R., & Tanna, H. (2005). The Lockheed-Georgia coannular jet research facility. The Journal of the Acoustical Society of America, *65*(S1), S44.

Cumpsty, N. A., & Whitehead, D. S. (1971). The excitation of acoustic resonances by vortex shedding. Journal of Sound and Vibration, *18*(3), 353–369. https://doi.org/10.1016/0022-460x(71)90707-3Karon, A. Z. (2016). Potential factors responsible for discrepancies in jet noise measurements of different studies [Ph.D. thesis, Daniel Guggenheim School of Aerospace Engineering, Georgia Institute of Technology].

Lepicovsky, J., & Ahuja, K. K. (1985). Experimental results on edge-tone oscillations in high-speed subsonic jets. AIAA Journal, *23*(10), 1463-1468.

Lepicovsky, J., Ahuja, K. K., & Burrin, R. H. (1985). Tone excited jets - part III: Flow measurements. Journal of Sound and Vibration, *102*(1), 71-91.

Parker, R. & Stoneman, S. A. T. (1989). The excitation and consequences of acoustic resonances in enclosed fluid flow around solid bodies. Proceedings of the Institution of Mechanical Engineers, Part C: Mechanical Engineering Science, *203*(1), 9–19.

## Appendix A – Support from ASDL

During the period of performance, the engine cycle team has been working with the ASCENT Project 10 (A10) team's matched cycle and flowpath for the nine supersonic transports shown in
Figure. The A10 researchers developed/converged on a cycle for all nine SST vehicles, and a notional flowpath is shown in
Figure. The engine cycle team is interested in the mixer exit and nozzle configuration shown in the red dotted square in
Figure and blown up with dimensional references in
Figure. To provide engine operating conditions during takeoff to the rest of the ASCENT 59 team, an optimization of the takeoff trajectory must be performed. This optimization is performed with the NASA Flight Optimization System's (FLOPS) takeoff and landing module. Based on the engine cycle thermodynamic performance, the flowpath information, detailed takeoff and landing aerodynamics for each SST, a set of variables controlling the takeoff trajectory, including the percentage program lapse rate (PLR), is perturbed within a given range. The resulting trajectories and associated certification noise levels are recorded. This dataset is examined to choose a trajectory with the lowest certification noise level subject to safety constraints. The resulting cycle conditions, mixer, and nozzle operating conditions for all nine configurations are shown in Tables A-1 to A-3. The variation (i.e., ranges) in these parameters for each class of SSTs is shown in cycle and dimensions in Tables A-4 to A-6. The variation in these parameters across all nine SSTs is shown in

**Table**.

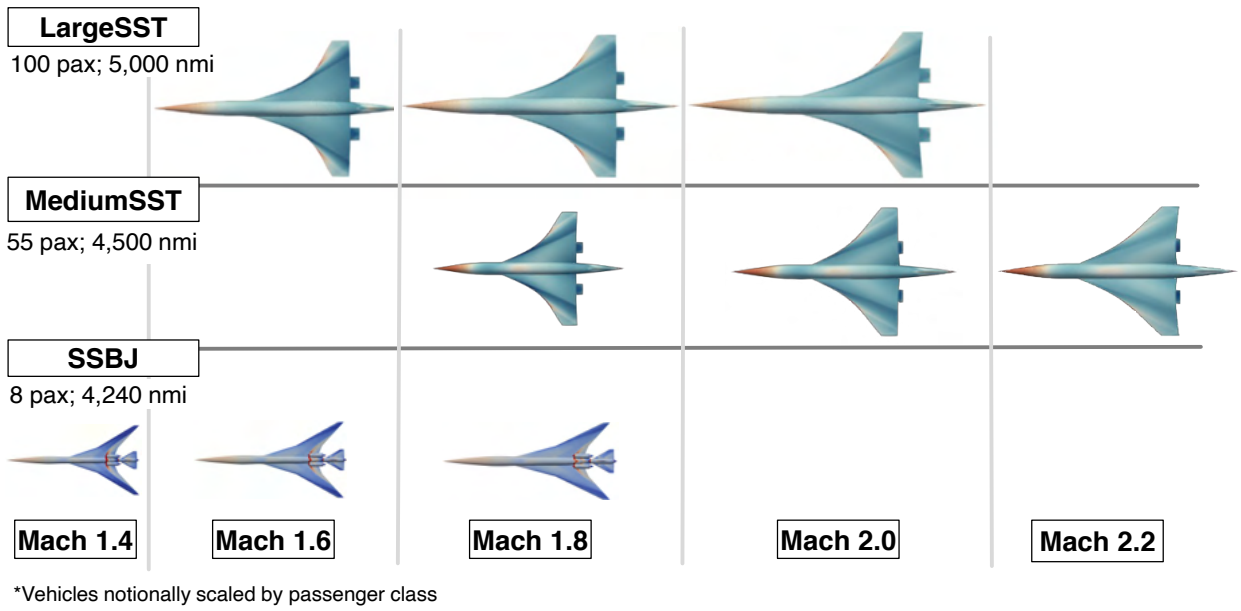


**Figure A-1.** Nine SST Configurations from ASCENT Project 10.

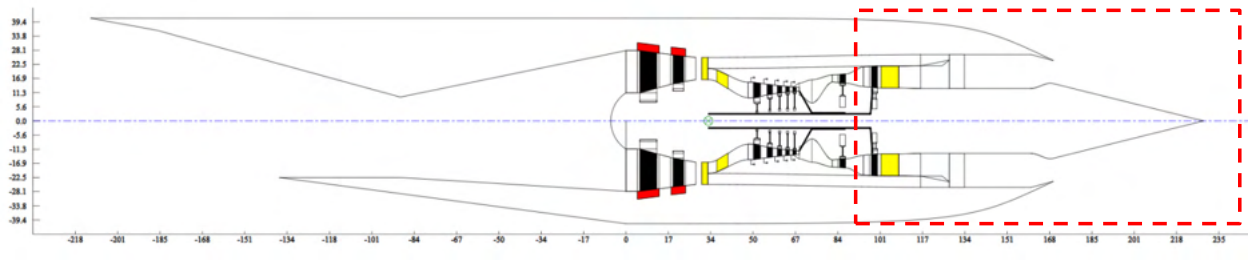

**Figure A-2.** Notional SST Flowpath.

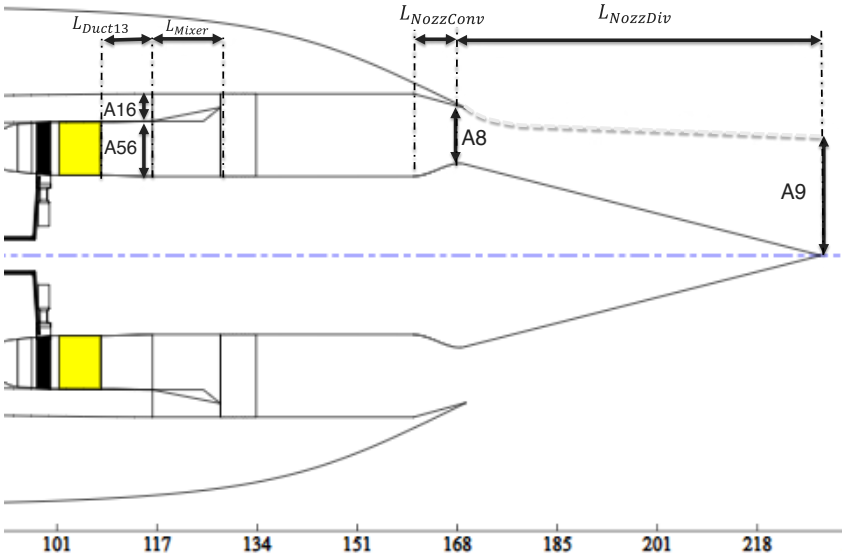


**Figure A-3.** Mixer and nozzle dimensional reference.

**Table A-1.** Cycle, mixer, and nozzle operating conditions during takeoff for three SSBJs.

| **Cycle Parameter @ TO, ISA+18F** | **SSBJ M1.4 (v1.5)** | | | **SSBJ M1.6 (v1.5)** | | | **SSBJ M1.8 (v1.5)** | | |
|---|---|---|---|---|---|---|---|---|---|
| BPR | 3.68 | | | 3.45 | | | 3.66 | | |
| FPR | 2.03 | | | 2.02 | | | 2.03 | | |
| NPR | 1.86 | | | 1.85 | | | 1.90 | | |
| Extraction Ratio | 1.11 | | | 1.10 | | | 1.05 | | |
| Duct 13 Length (in) | 5.00 | | | 5.00 | | | 5.00 | | |
| Mixer Length (in) | 10.19 | | | 10.74 | | | 11.34 | | |
| Nozzle Converg. Length (in) | 9.76 | | | 11.22 | | | 12.77 | | |
| Nozzle Diverg. Length (in) | 53.54 | | | 58.82 | | | 63.72 | | |
| Station | Area [sq. in] | Mach | Tt [deg R] | Area [sq. in] | Mach | Tt [deg R] | Area [sq. in] | Mach | Tt [deg R] |
| 16 (Mixer secondary in) | 812.2 | 0.560 | 680.7 | 889.4 | 0.548 | 679.7 | 1055.7 | 0.476 | 680.6 |
| 5.6 (Mixer primary in) | 519.1 | 0.407 | 1773.1 | 590.5 | 0.406 | 1749.8 | 592.6 | 0.405 | 1861.6 |
| 6 (Mixer out) | 1331.3 | 0.527 | 934.9 | 1479.9 | 0.518 | 940.9 | 1648.3 | 0.479 | 959.2 |
| 7 (Nozzle in) | 1331.3 | 0.543 | 934.9 | 1479.9 | 0.534 | 940.9 | 1648.3 | 0.492 | 959.2 |
| 8 (Nozzle throat) | 1082.8 | 0.987 | 934.9 | 1189.2 | 0.985 | 940.9 | 1254.9 | 1.000 | 959.2 |
| 9 (Nozzle out) | 1051.0 | 0.987 | 934.9 | 1154.6 | 0.985 | 940.9 | 1214.8 | 1.004 | 959.2 |

**Table A-2.** Cycle, mixer, and nozzle operating conditions during takeoff for three medium SSTs.

| **Cycle Parameter @ TO, ISA+18F** | **Medium SST M1.8 (v12.2)** | | | **Medium SST M2.0 (v12.2)** | | | **Medium SST M2.2 (v12.2)** | | |
|---|---|---|---|---|---|---|---|---|---|
| BPR | 3.38 | | | 2.93 | | | 2.58 | | |
| FPR | 2.02 | | | 2.10 | | | 2.20 | | |
| NPR | 1.89 | | | 1.98 | | | 2.09 | | |
| Extraction Ratio | 1.06 | | | 1.04 | | | 1.02 | | |
| Duct 13 Length (in) | 5.00 | | | 5.00 | | | 5.00 | | |
| Mixer Length (in) | 12.50 | | | 13.30 | | | 13.59 | | |
| Nozzle Converg. Length (in) | 13.47 | | | 16.16 | | | 18.50 | | |
| Nozzle Diverg. Length (in) | 68.74 | | | 77.43 | | | 83.87 | | |
| Station | Area [sq. in] | Mach | Tt [deg R] | Area [sq. in] | Mach | Tt [deg R] | Area [sq. in] | Mach | Tt [deg R] |
| 16 (Mixer secondary in) | 1237.3 | 0.487 | 680.0 | 1363.0 | 0.457 | 688.4 | 1389.6 | 0.430 | 698.9 |
| 5.6 (Mixer primary in) | 767.1 | 0.405 | 1824.6 | 904.1 | 0.404 | 1813.1 | 980.1 | 0.405 | 1833.0 |
| 6 (Mixer out) | 2004.4 | 0.483 | 967.3 | 2267.1 | 0.462 | 1001.6 | 2369.8 | 0.445 | 1044.3 |
| 7 (Nozzle in) | 2004.4 | 0.497 | 967.3 | 2267.1 | 0.475 | 1001.6 | 2369.8 | 0.457 | 1044.3 |
| 8 (Nozzle throat) | 1535.2 | 1.000 | 967.3 | 1688.0 | 1.000 | 1001.6 | 1716.5 | 1.000 | 1044.3 |
| 9 (Nozzle out) | 1486.4 | 1.003 | 967.3 | 1627.0 | 1.043 | 1001.6 | 1659.4 | 1.086 | 1044.3 |

**Table A-3.** Cycle, mixer, and nozzle operating conditions during takeoff for three large SSTs.

| **Cycle Parameter @ TO, ISA+18F** | **Large SST M1.6 (v1.2)** | | | **Large SST M1.8 (v1.2)** | | | **Large SST M2.0 (v1.2)** | | |
|---|---|---|---|---|---|---|---|---|---|
| BPR | 3.73 | | | 3.37 | | | 2.87 | | |
| FPR | 2.07 | | | 2.08 | | | 2.20 | | |
| NPR | 1.92 | | | 1.94 | | | 2.06 | | |
| Extraction Ratio | 1.07 | | | 1.05 | | | 1.03 | | |
| Duct 13 Length (in) | 5.00 | | | 5.00 | | | 5.00 | | |
| Mixer Length (in) | 14.07 | | | 14.89 | | | 15.00 | | |
| Nozzle Converg. Length (in) | 13.63 | | | 16.04 | | | 18.71 | | |
| Nozzle Diverg. Length (in) | 73.55 | | | 81.68 | | | 88.44 | | |
| Station | Area [sq. in] | Mach | Tt [deg R] | Area [sq. in] | Mach | Tt [deg R] | Area [sq. in] | Mach | Tt [deg R] |
| 16 (Mixer secondary in) | 1596.8 | 0.503 | 685.2 | 1759.7 | 0.476 | 686.3 | 1725.9 | 0.446 | 698.8 |
| 5.6 (Mixer primary in) | 941.3 | 0.405 | 1888.2 | 1083.0 | 0.405 | 1886.3 | 1157.4 | 0.405 | 1890.7 |
| 6 (Mixer out) | 2538.1 | 0.496 | 966.7 | 2842.7 | 0.478 | 989.4 | 2883.3 | 0.457 | 1037.7 |
| 7 (Nozzle in) | 2538.1 | 0.511 | 966.7 | 2842.7 | 0.491 | 989.4 | 2883.3 | 0.469 | 1037.7 |
| 8 (Nozzle throat) | 1986.3 | 1.000 | 966.7 | 2165.0 | 1.000 | 989.4 | 2131.6 | 1.000 | 1037.7 |
| 9 (Nozzle out) | 1920.5 | 1.014 | 966.7 | 2090.9 | 1.024 | 989.4 | 2058.1 | 1.076 | 1037.7 |

**Table A-4.** Variations in cycle, mixer, and nozzle operating conditions for SSBJs (v1.5).

| **Cycle Parameter** | **SSBJ (v1.5) Ranges** | | | | | |
|---|---|---|---|---|---|---|
| **@ TO, ISA+18F** | Low | High | | | | |
| BPR | 3.45 | 3.68 | | | | |
| FPR | 2.02 | 2.03 | | | | |
| NPR | 1.85 | 1.90 | | | | |
| Extraction Ratio | 1.05 | 1.11 | | | | |
| Duct 13 Length (in) | 5.00 | 5.00 | | | | |
| Mixer Length (in) | 10.19 | 11.34 | | | | |
| Nozzle Converg. Length (in) | 9.76 | 12.77 | | | | |
| Nozzle Diverg. Length (in) | 53.54 | 63.72 | | | | |
| Station | Area (sq. in) [Low - High] | | Mach [Low - High] | | Tt (deg R) [Low - High | |
| 16 (Mixer secondary in) | 812.2 | 1055.7 | 0.476 | 0.560 | 679.730 | 680.7 |
| 5.6 (Mixer primary in) | 519.1 | 592.6 | 0.405 | 0.407 | 1749.750 | 1861.6 |
| 6 (Mixer out) | 1331.3 | 1648.3 | 0.479 | 0.527 | 934.890 | 959.2 |
| 7 (Nozzle in) | 1331.3 | 1648.3 | 0.492 | 0.543 | 934.890 | 959.2 |
| 8 (Nozzle throat) | 1082.8 | 1254.9 | 0.985 | 1.000 | 934.890 | 959.2 |
| 9 (Nozzle out) | 1051.0 | 1214.8 | 0.985 | 1.004 | 934.890 | 959.2 |

**Table A-5.** Variations in cycle, mixer, and nozzle operating conditions for medium SSTs (v12.2).

| **Cycle Parameter** | **Medium SST (v12.2) Ranges** | | | | | |
|---|---|---|---|---|---|---|
| **@ TO, ISA+18F** | Low | High | | | | |
| BPR | 2.58 | 3.38 | | | | |
| FPR | 2.02 | 2.20 | | | | |
| NPR | 1.89 | 2.09 | | | | |
| Extraction Ratio | 1.02 | 1.06 | | | | |
| Duct 13 Length (in) | 5.00 | 5.00 | | | | |
| Mixer Length (in) | 12.50 | 13.59 | | | | |
| Nozzle Converg. Length (in) | 13.47 | 18.50 | | | | |
| Nozzle Diverg. Length (in) | 68.74 | 83.87 | | | | |
| Station | Area (sq. in) [Low - High] | | Mach [Low - High] | | Tt (deg R) [Low - High | |
| 16 (Mixer secondary in) | 1237.3 | 1389.6 | 0.430 | 0.487 | 679.980 | 698.9 |
| 5.6 (Mixer primary in) | 767.1 | 980.1 | 0.404 | 0.405 | 1813.120 | 1833.0 |
| 6 (Mixer out) | 2004.4 | 2369.8 | 0.445 | 0.483 | 967.270 | 1044.3 |
| 7 (Nozzle in) | 2004.4 | 2369.8 | 0.457 | 0.497 | 967.270 | 1044.3 |
| 8 (Nozzle throat) | 1535.2 | 1716.5 | 1.000 | 1.000 | 967.270 | 1044.3 |
| 9 (Nozzle out) | 1486.4 | 1659.4 | 1.003 | 1.086 | 967.270 | 1044.3 |

**Table A-6.** Variations in cycle, mixer, and nozzle operating conditions for large SSTs (v1.2).

| **Cycle Parameter** | **Large SST (v1.2) Ranges** | | | | | |
|---|---|---|---|---|---|---|
| **@ TO, ISA+18F** | Low | High | | | | |
| BPR | 2.87 | 3.73 | | | | |
| FPR | 2.07 | 2.20 | | | | |
| NPR | 1.92 | 2.06 | | | | |
| Extraction Ratio | 1.03 | 1.07 | | | | |
| Duct 13 Length (in) | 5.00 | 5.00 | | | | |
| Mixer Length (in) | 14.07 | 15.00 | | | | |
| Nozzle Converg. Length (in) | 13.63 | 18.71 | | | | |
| Nozzle Diverg. Length (in) | 73.55 | 88.44 | | | | |
| Station | Area (sq. in) [Low - High] | | Mach [Low - High] | | Tt (deg R) [Low - High | |
| 16 (Mixer secondary in) | 1596.8 | 1759.7 | 0.4 | 0.5 | 685.2 | 698.8 |
| 5.6 (Mixer primary in) | 941.3 | 1157.4 | 0.405 | 0.405 | 1886.320 | 1890.7 |
| 6 (Mixer out) | 2538.1 | 2883.3 | 0.457 | 0.496 | 966.740 | 1037.7 |
| 7 (Nozzle in) | 2538.1 | 2883.3 | 0.469 | 0.511 | 966.740 | 1037.7 |
| 8 (Nozzle throat) | 1986.3 | 2165.0 | 1.000 | 1.000 | 966.740 | 1037.7 |
| 9 (Nozzle out) | 1920.5 | 2090.9 | 1.014 | 1.076 | 966.740 | 1037.7 |

**Table A-7.** Variations in cycle, mixer, and nozzle operating conditions across all nine SSTs.

| **Cycle Parameter** | **Ranges over all 9 configurations** | | | | | |
|---|---|---|---|---|---|---|
| **@ TO, ISA+18F** | Low | High | | | | |
| BPR | 2.58 | 3.73 | | | | |
| FPR | 2.02 | 2.20 | | | | |
| NPR | 1.85 | 2.09 | | | | |
| Extraction Ratio | 1.02 | 1.11 | | | | |
| Duct 13 Length (in) | 5.00 | 5.00 | | | | |
| Mixer Length (in) | 10.19 | 15.00 | | | | |
| Nozzle Converg. Length (in) | 9.76 | 18.71 | | | | |
| Nozzle Diverg. Length (in) | 53.54 | 88.44 | | | | |
| Station | Area (sq. in) [Low - High] | | Mach [Low - High] | | Tt (deg R) [Low - High | |
| 16 (Mixer secondary in) | 812.2 | 1759.7 | 0.4 | 0.6 | 679.7 | 698.9 |
| 5.6 (Mixer primary in) | 519.1 | 1157.4 | 0.404 | 0.407 | 1749.750 | 1890.7 |
| 6 (Mixer out) | 1331.3 | 2883.3 | 0.445 | 0.527 | 934.890 | 1044.3 |
| 7 (Nozzle in) | 1331.3 | 2883.3 | 0.457 | 0.543 | 934.890 | 1044.3 |
| 8 (Nozzle throat) | 1082.8 | 2165.0 | 0.985 | 1.000 | 934.890 | 1044.3 |
| 9 (Nozzle out) | 1051.0 | 2090.9 | 0.985 | 1.086 | 934.890 | 1044.3 |